Oxidation of MnO(100) and $NaMnO_2$ formation: Characterization of Mn^{2+} and Mn^{3+} Surfaces via XPS and Water TPD

Xu Feng , David F. Cox

PII: S0039-6028(18)30154-7
DOI: 10.1016/j.susc.2018.04.022
Reference: SUSC 21247

To appear in: *Surface Science*

Received date: 14 February 2018
Revised date: 27 April 2018
Accepted date: 29 April 2018

Please cite this article as: Xu Feng , David F. Cox , Oxidation of MnO(100) and $NaMnO_2$ formation: Characterization of Mn^{2+} and Mn^{3+} Surfaces via XPS and Water TPD, *Surface Science* (2018), doi: 10.1016/j.susc.2018.04.022

Highlights

Mn_3O_4-like and Mn_2O_3-like surfaces can be formed in UHV by the oxidation with O_2 of the clean and nearly-stoichiometric MnO(100).

• A $NaMnO_2$-like surface can be produced by oxidation of the MnO(100) pre-covered with multilayers of metallic Na.

• Water is sensitive to the Mn oxidation state, and desorbs at different temperatures from the manganese oxide surfaces dependent on the Mn oxidation state.

• On the $NaMnO_2$-like surface, pre-adsorbed water blocks the uptake of CO_2, and water displaces pre-adsorbed CO_2.

Oxidation of MnO(100) and $NaMnO_2$ formation: Characterization of Mn^{2+} and Mn^{3+} Surfaces via XPS and Water TPD

Xu Feng and David F. Cox

Department of Chemical Engineering, Virginia Polytechnic Institute and State University, Blacksburg, VA 24061

* corresponding author: dfcox@vt.edu

Keywords: manganese oxide, $NaMnO_2$, water, carbon dioxide, X-ray photoelectron spectroscopy, temperature programmed desorption, low energy electron diffraction

ABSTRACT

The oxidation of clean and Na precovered MnO(100) has been investigated by X-ray photoelectron spectroscopy (XPS), low energy electron diffraction (LEED) and temperature programmed desorption (TPD) of adsorbed water. XPS results indicate that Mn_3O_4-like and Mn_2O_3-like surfaces can be formed by various oxidation treatments of clean and nearly-stoichiometric MnO(100), while a $NaMnO_2$-like surface can be produced by the oxidation of MnO(100) pre-covered with multilayers of metallic Na. Water TPD results indicate that water adsorption/desorption is sensitive to the available oxidation states of surface Mn cations, and can be used to distinguish between surfaces exposing $Mn^{2+}$and Mn^{3+} cations, or a combination of these oxidation states. Carbon dioxide and water TPD results from the $NaMnO_2$-like surface indicate that pre-adsorbed water blocks the uptake of CO_2, while water displaces pre-adsorbed CO_2. No indication of a strong reactive interaction is observed between CO_2, water and the $NaMnO_2$-like surface under the conditions of our study.

1. Introduction

$NaMnO_2$ has been studied primary in electrochemistry as a novel cathode material for lithium/sodium-ion batteries because of its competitive ability for the intercalation and de-intercalation of Na [1, 2]. For these investigations, the first and critical step is the synthesis of $NaMnO_2$. Ma, Chen and Cedar [2] synthesized $NaMnO_2$ via a solid-state reaction of stoichiometric amounts of Na_2CO_3 and Mn_2O_3 powders. Parant *et al.* [3] grew $NaMnO_2$ single crystals by a solid state reaction of Na_2O_2 with MnO. Hirano, Narita and Naka [4] synthesized single crystals of $Na_{0.70}MnO_{2+y}$ ($0 \leq y \leq 0.25$) via hydrothermal synthesis starting from various manganese oxides and sodium hydroxide solutions. However there is no report of the formation and characterization of a $NaMnO_2$ surface in a well-defined model system, which is desirable in order to understand the basic structural and electronic properties of $NaMnO_2$ and its interfacial behavior in electrochemistry.

In recent years, $NaMnO_2$ has also gained interests in catalysis. Xu, Bhawe and Davis [5] reported a low-temperature, manganese-oxide-based, catalytic thermochemical water splitting cycle. In this complex system, the redox reactions of Mn^{2+}/Mn^{3+} oxides play important roles in the water splitting cycle. In the hydrogen evolution steps, water reacts with a Na_2CO_3/MnO mixture to produce hydrogen and release CO_2, while Na^+ intercalates into MnO to form α-$NaMnO_2$ where Mn^{2+} is oxidized to Mn^{3+}. In the catalyst recovery steps, aqueous CO_2 at 80 ºC is used to facilitate the removal of Na^+ from α-$NaMnO_2$. Water intercalation into this layered compound increases the mobility of Na^+ and leads to the formation of Na_2CO_3 and birnessite-type manganese oxides ($H_xMnO_2 \cdot yH_2O$). The remaining manganese compound then thermally reduced from Mn^{3+} to Mn^{2+}. Therefore, a study of the formation and redox cycles of MnO and $NaMnO_2$ may provide insight into the fundamental steps in this innovative water splitting cycle.

A number of studies have been reported for the formation of manganese oxides with various Mn oxidation states from 2+ (MnO) to 4+ (MnO_2) from the oxidation of manganese powder or metal films [6-9]. X-ray photoelectron spectroscopy (XPS) was used to characterize various Mn oxidation states by using the Mn $2p_{3/2}$ binding energy and the Mn 3s splitting. Despite a wide range of overlapping values reported for the Mn $2p_{3/2}$ binding energy and Mn 3s splitting for various manganese oxides, a higher Mn $2p_{3/2}$ binding energy and a weaker Mn 3s splitting are commonly observed for higher Mn oxidation states.

A few studies have been reported for the oxidation of well-ordered MnO(100) surfaces to higher-valence manganese oxides [10, 11]. Bayer *et al.* [10] produced an ordered Mn_3O_4(001) surface by oxidizing a Pd(100)-supported MnO(001) thin film. Langell *et al.* [11] performed the Mn^{2+}/Mn^{3+} redox cycle by the oxidation of a MnO(100) single crystal surface to Mn_2O_3, with subsequent thermal reduction to Mn_3O_4 and MnO(100).

In this work, we start from the oxidation of a clean MnO(100) surface to produce Mn_3O_4- and Mn_2O_3-like surfaces, then we investigate the oxidation of Na-precovered MnO(100) and report the first $NaMnO_2$-like surface formed on a MnO(100) substrate. X-ray photoelectron spectroscopy (XPS) was used to characterize and compare changes in chemical states of the surface elements (Na, Mn and O) and surface composition of the formed manganese oxide and $NaMnO_2$ surfaces. In addition, water was used as a probe molecule in temperature programmed desorption (TPD) to further distinguish the formed manganese oxide and $NaMnO_2$ surfaces. TPD of CO_2 and water on the $NaMnO_2$-like surface was examined for any insight into the mechanism of Na^+ extraction from $NaMnO_2$ by aqueous CO_2.

2. Model Surface: MnO(100)

Fig.1 shows a ball model illustration of an ideal stoichiometric MnO(100) surface, with atom sizes referenced to Mn and O bonded radii [12]. MnO has the simple rocksalt structure [13]. In the bulk, each Mn^{2+} cation is surrounded by six equidistant O^{2-} anions, while each O^{2-} anion is surrounded by six equidistant Mn^{2+} cations. The crystal structure of MnO can be considered as the insertion of two fcc lattices of Mn^{2+} and O^{2-} ions [14]. The non-polar MnO(100) surface has the lowest surface energy among all the low miller-index surfaces, and is thermodynamically stable [13]. An ideal (100) surface exposes an atomically flat plane containing equal numbers of Mn^{2+} cations and O^{2-} anions with a square periodicity (a:b = 1:1), however in practice, surface defects such as steps, kinks, missing ions or adatoms (or ions) cannot be avoided [13]. The clean MnO(100) surface shows very little rumpling or reconstruction in the ultra-high vacuum environment [11, 15].

3. Experimental

All experiments were carried out in a turbo-pumped, dual-chamber, stainless steel ultra-high vacuum (UHV) system. The preparation chamber with a base pressure of 2×10^{-10} Torr is equipped with a Leybold IQE 10/35 ion gun, a set of Princeton Research Instruments reverse view LEED optics and an Inficon Quaqrex 200 mass spectrometer for TPD. The analysis chamber with a base pressure of 1×10^{-10} Torr is equipped with a Leybold EA-11 hemispherical analyzer and a Mg Kα radiation source for XPS, and a Na evaporator with an SAES getter as the Na source.

The MnO(100) single crystal was purchased from SurfaceNet GmbH with an EPI polish. The sample was mechanically clamped onto a Ta stage that was fastened to LN_2-cooled copper electrical feedthroughs in a sample rod manipulator. The sample temperature was directly measured by a type K thermocouple attached to the back of the single crystal through a hole in

the Ta stage using Aremco 569 ceramic cement. The sample holder can be resistively heated to 1000 K and LN_2-cooled to 125 K. A low heating rate of 2.5 $K \cdot s^{-1}$ was used for TPD to avoid thermal-induced fracture of the ceramic MnO sample.

Na was evaporated onto the sample from a resistively heated Na SAES getter placed approximately 30 mm away from the sample. O_2 (Matheson, 99.998%) and CO_2 (Matheson, 99.999%) were used as received. D_2O (Sigma-Aldrich, 99.9 atom % D) was degassed by repeated freeze-pump-thaw cycles prior to use. Gases were introduced by backfilling the chamber through a variable leak valve, and the reported exposures have been corrected for an ion gauge sensitivity of 1.4 for CO_2 and 1.0 for O_2 and D_2O [16].

LEED was used to examine the surface long-range order at a temperature of 473 K, high enough to provide sufficient conductivity to this room temperature insulator to avoid surface charging [17]. XPS spectra were acquired at 60 eV pass energy for Mn, O and Na 1s which gives a Ag $3d_{5/2}$ line width of 1.06 eV, and 200 eV pass energy for Na KLL which gives a Ag $3d_{5/2}$ line width of 2.1 eV. All binding energies of the MnO(100), Mn_3O_4-like and Mn_2O_3-like surfaces have been referenced to an O 1s binding energy of 530.1 eV for the MnO(100) substrate using an approach similar to that of Langell *et al.* [11]. This value was obtained with clean MnO(100) at an elevated temperature of 473 K which provides sufficient conductivity to eliminate surface charging. Similarly, binding energies of the $NaMnO_2$-like surface have been referenced to the O 1s binding energy value obtained with the $NaMnO_2$-like surface at an elevated temperature of 473 K where a value of 530.1 eV is also found.

Reported values for XPS O/Mn and O/Na ratios are determined from the integrated intensity of the O 1s, Mn 2p and Na 1s photoemission features following satellite and Shirley background [18] subtraction. All XPS ratios have been corrected by atomic sensitivity factors

except where noted. The ratio of XPS atomic sensitivity factors are estimated by $\frac{S_1}{S_2} \approx \frac{\sigma_1 \lambda_1 / KE_1}{\sigma_2 \lambda_2 / KE_2}$ as described elsewhere [19, 20], where σ is the photoionization cross section of the element core level found in published data [21], *KE* is the kinetic energy of the photoemitted electron, and λ is the inelastic mean free path of the photoemitted electron. Mean free paths have been estimated by a predictive formula (TPP-2M equation [22, 23]) in the NIST Electron Inelastic-Mean-Free-Path Database [24]. A detailed description of methods used to calculate the ratios of XPS atomic sensitivity factor can be found in the supplementary material. All XPS spectra shown in the figures have been corrected by satellite subtraction, but no background corrections have been applied.

4. Results and Discussion

4.1. Oxidation of clean MnO(100): Formation of Mn_3O_4 and Mn_2O_3

A clean and nearly-stoichiometric MnO(100) surface was prepared by 2 keV Ar^+ ion bombardment at room temperature and annealing to 1000 K in UHV as reported elsewhere [17]. After the preparation procedure, the sample exhibits a sharp (1×1) LEED pattern characteristic of a simple termination of the rocksalt-structured (cubic) MnO bulk [17]. As shown in Fig. 2(a), this surface gives a Mn $2p_{3/2}$ binding energy of 641.1 eV, with a shake-up satellite feature at 6.2 eV higher binding energy. Both values are in good agreement with previous reports for a clean and stoichiometric MnO(100) surface [11]. A Mn 3s splitting of 6.1 eV is observed, which also agrees with values reported for MnO [6, 8, 9, 25-28].

The O 1s to Mn 2p XPS integrated intensity ratio is used to estimate the surface composition. XPS for the as-prepared surface gives an *uncorrected* O 1s to Mn 2p intensity ratio of 0.24, which matches the value for a clean and stoichiometric MnO(100) surface reported by

Langell *et al.* [11] using a different preparation method. After correction with standard empirical XPS atomic sensitivity factors for our analyzer, the experimental O 1s/Mn 2p ratio is 1.20, 20% greater than the ideal 1:1 stoichiometry for the MnO bulk. However, given the different kinetic energies of the Mn and O photoelectron and hence the inelastic mean free path, deviations from the bulk composition are not unexpected for a single crystal compound surface [19].

A conventional layer-by-layer summation was used to simulate the expected O/Mn ratio for an ideal MnO(100) surface [19]. This method assumes an exponential decay of signal intensity with distance into the bulk for normal emission, and no diffraction effects. The inelastic mean free paths of Mn and O in MnO were predicted using the NIST Electron Inelastic-Mean-Free-Path Database [24] as described in the experimental section. This simulation gives an O/Mn ratio of 1.15, which is close to the experimental value of 1.20.

Various oxidation treatments on the clean MnO(100) surface result in the formation of Mn_3O_4-like and Mn_2O_3-like surfaces as characterized by XPS. Di Castro and Polzonetti [9] oxidized MnO layers to Mn_2O_3 by annealing in 1 atm of O_2 at 673 K for 15 min without the intermediate formation of Mn_3O_4. Langell *et al.* [11] reported the formation of a Mn_2O_3 surface by annealing a MnO(100) single crystal surface in 5×10^{-7} Torr of O_2 at 625 K for 2.5 h. We have repeated their preparation procedures (5×10^{-7} - 1×10^{-6} Torr O_2, 625 - 673 K, up to 2.5 h) but fail to obtain a Mn_2O_3-like surface. Instead, we find Mn_3O_4-like surfaces as characterized by XPS. We find that annealing the MnO(100) surface in 1×10^{-6} Torr of O_2 at 673 K for 15 min is sufficient to form the Mn_3O_4-like surface as characterized by XPS and shown in Fig. 2(b). The Mn $2p_{3/2}$ binding energy of 641.8 eV is 0.7 eV higher than MnO(100), indicating the presence of higher Mn oxidation states than for MnO alone (2+) [6, 7, 9]. This result is consistent with the expected mixed Mn oxidation states of 2+ and 3+ for Mn_3O_4. The measured Mn $2p_{3/2}$ peak width

(FWHM = 4.0 eV) is broadened by 0.3 eV compared to MnO(100) (3.7 eV), which may be attributed to the co-existence of two Mn oxidation states. The previously observed shake-up satellite feature for MnO disappears, consistent with literature reports for Mn_3O_4 that the satellite shifts to higher binding energies and overlaps with the Mn $2p_{1/2}$ feature (not shown) [9, 11, 26]. The Mn 3s splitting decreases to 5.6 eV, also in agreement with values reported for Mn_3O_4 [6, 9], indicating the presence of Mn^{3+}. No obvious differences in the characteristics of the O 1s binding energy (530.1 eV) or peak width (2.0 eV) are observed compared to MnO(100). The *uncorrected* O 1s/Mn 2p XPS intensity ratio for this surface is 1.55, which is 29% greater than the value observed for near ly-stoichiometric MnO(100). This increase is close to the ideal 33% increase of the O/Mn ratio expected for a stoichiometry change from MnO to Mn_3O_4. Only a diffuse background is observed in LEED, indicating that the structure of this oxidized surface has no long-range periodicity.

In order to further oxidize Mn_3O_4 to Mn_2O_3, a mild ion bombardment followed by a UHV annealing was used to generate surface defects as an attempt to facilitate further oxidation before additional annealing in O_2. It is found that a Mn_2O_3-like surface, as characterized by XPS, could be formed by repeatedly treating a Mn_3O_4-like surface by ion bombardment at room temperature (Ar^+ bombardment, 500 eV), UHV annealing to 1000 K for 10 min, then annealing in 1×10^{-6} Torr of O_2 at 673 K for 15 min and 625 K for 2 h. Here we need to note that this method did not always give a reproducible surface composition. Fig. 2(c) shows the XPS spectra of a Mn_2O_3-like surface formed by this procedure. Similar to the Mn_3O_4-like surface, the Mn $2p_{3/2}$ binding energy of 641.8 eV and the absence of the shake-up satellite feature both indicate the presence of Mn^{3+}. However, with the exception of surface composition, the characteristics of the XPS signals are essentially indistinguishable between the Mn_2O_3-like and Mn_3O_4-like surfaces. The

uncorrected O 1s/Mn 2p XPS intensity ratio for the Mn_2O_3-like surface in Fig. 2(c) is 1.85 and is 54% greater than that observed for MnO(100). This increase is close to the ideal 50% increase expected in the O/Mn ratio for a stoichiometry change from MnO to Mn_2O_3. Similar to the Mn_3O_4-like surface, only a diffuse background is observed in LEED, indicating that the structure of this oxidized surface has no long-range periodicity. We note that our data do not provide a good indication of the thickness of the Mn_3O_4 and Mn_2O_3 surfaces prepared by our oxidation treatments. However, the similarity in measured compositions to those expected for the stoichiometric materials suggests the thickness of the oxidized layers are at least on the order of the XPS sampling depth.

4.2. Oxidation Na-precovered MnO(100): Formation of $NaMnO_2$

Parant *et al.* [3] have synthesized $NaMnO_2$ crystals via a solid state reaction between MnO and sodium oxide. A similar approach was envisioned here where metallic Na deposited on the MnO(100) surface is oxidized to generate a Na oxide overlayer that can react with the underlying MnO(100) substrate. Since Na_2O decomposes at 800K in UHV during TPD [29], flashing the sample to 1000K in UHV following the oxidation treatment will remove any excess Na oxide not used for the bimetallic compound formation.

Fig. 3(a) shows the XPS spectra of a MnO(100) surface pre-covered with 11.5 ML of Na. The method used for the Na coverage determination and a description of the interactions between Na and MnO(100) in a non-oxidizing environment are reported elsewhere [17]. The appearance of plasmon loss features in both the Na 1s and Na KLL spectra indicates the dominant presence of metallic Na on MnO(100) at this coverage [30-33]. While the Mn and O XPS signals are greatly attenuated by the Na overlayer, the binding energies of $Mn2p_{3/2}$ and O1s, the peak width of $Mn2p_{3/2}$, and the Mn 3s splitting are similar to those of clean MnO(100).

A $NaMnO_2$-like surface was produced by annealing the 11.5 ML Na-precovered MnO(100) surface in 1×10^{-6} Torr of O_2 at 673 K for 15 min, then briefly heating (flash) to 1000 K in UHV. This surface is characterized by XPS as shown in Fig. 3(b). The plasmon loss features are absent in both Na 1s and Na KLL spectra, indicating that metallic Na is no longer present. Na KLL shows a single peak, indicating Na in the form of a non-metallic Na compound [30, 32-34]. A Na 1s peak at 1071.2 eV is observed, which is 0.2 eV lower than that for metallic Na. In our previous work of Na deposition on MnO(100) [17], we found that oxidic Na on the MnO substrate exhibits higher Na 1s binding energy than that for metallic Na, as would be normally expected. Nonetheless, although unexpected, the Na 1s binding energy of several bimetallic sodium oxides, such as $NaCrO_4$, $NaAsO_2$ and Na_2SeO_3, are reported to be 0.1 - 0.9 eV lower than that for metallic Na [34]. Due to the lack of reported data for $NaMnO_2$, here we consider the measured Na 1s binding energy of $NaMnO_2$ to be consistent with those reported for other bimetallic sodium oxides. Additional support for this assignment can be found in the supplementary material where the Na Auger parameter from this work is compared to other bimetallic sodium oxides on a Wagner plot. The Mn $2p_{3/2}$ binding energy is 641.9 eV with the absence of a shake-up satellite feature, and the Mn 3s splitting of this surface is 5.5 eV, which are all similar to those for the Mn_3O_4-like and Mn_2O_3-like surface and indicate the presence of Mn^{3+}. This result is in agreement with the expected Mn oxidation state (3+) in $NaMnO_2$ [35]. The peak width (FWHM) of Mn $2p_{3/2}$ is 3.4 eV, narrower than both clean (3.7 eV) and oxidized (4.0 eV) MnO(100), and the O 1s signal for this surface has a similar binding energy (530.1 eV) but a narrower peak width (1.6 eV) compared to those for the clean and oxidized MnO(100). The increased Mn intensity following oxidation of the deposited Na layer suggests that the remaining sodium intermixes with the underlying substrate rather than remaining as a sodium oxide over

layer. The surface composition estimated by XPS gives a Na:Mn:O XPS intensity ratio of 1.19:0.93:2 using atomic sensitivity factors estimated specifically for $NaMnO_2$ (see supplemental material). This surface composition is close to that expected for $NaMnO_2$, and indicates a film of the bimetallic oxide at least as thick as the XPS sampling depth. Similar to the Mn_3O_4-like and Mn_2O_3-like surfaces, only a diffuse background is observed in LEED, indicating that the structure of this surface has no long-range periodicity. While we start with a well-defined substrate, the resulting film is not structurally well-defined since epitaxial growth is not achieved.

Prolonged annealing (> 10 min) of the $NaMnO_2$-like surface in UHV at 1000 K results in the reduction of Mn as shown in Fig. 3(c). The Mn $2p_{3/2}$ binding energy (641.1 eV) and peak width (3.7 eV), the presence of shake-up satellite feature, and the Mn 3s splitting (6.0 eV) are all similar to those for the clean MnO(100) and characteristic of Mn^{2+}. These results indicate that Mn^{3+} in $NaMnO_2$ is reduced to Mn^{2+} by the thermal treatment in UHV of the $NaMnO_2$-like surface. Na 1s and Na KLL signals are significantly attenuated with no Na desorption signal (m/z = 23) detected in TPD. Similar observations were reported in our previous work of Na deposition on MnO(100) [17] at elevated temperatures in UHV, and are attributed to the thermally-induced inward diffusion of adsorbed Na.

4.3. D_2O TPD

Water was used as a probe molecule to examine and further distinguish the clean and oxidized MnO(100) surfaces and the $NaMnO_2$-like surface. Fig. 4 shows the TPD traces of D_2O (m/z = 20) following 0.5 L (1 L ≡ 1×10^{-6} Torr·s) D_2O dose on the four surfaces. For each dose, the surface was cooled to 125 K prior to dosing, and TPD was run for the temperature range from 125 K to 600 K. For clean MnO(100) exposing cations in a 2+ oxidation state, the main D_2O desorption feature is observed below 300 K with a peak maximum at 230 K as shown in Fig.

4(a). Water desorption features in a similar temperature range are reported on other rocksalt-structured metal oxide surfaces such as MgO(100) [36, 37] and NiO(100) [38, 39], and have been attributed to molecularly adsorbed water on terrace sites. The high temperature tail of the water desorption peak above 300 K is assigned to the recombination of dissociated water in agreement with most literature reports [40, 41].

Fig. 4(b) shows the water TPD traces on the Mn_3O_4-like surface. Similar to MnO(100), water desorbs primarily below 300 K. However two desorption features are observed at 195 K and 235 K, suggesting that two types of water adsorption sites are present. The desorption peak at 235 K is at a similar temperature to the main water desorption peak on the MnO(100) surface (Mn^{2+}), suggesting that it may be associated with surface Mn^{2+} in Mn_3O_4. The other water desorption feature appears at lower temperature (195 K), suggesting that water binds more weakly on a second type of adsorption site.

On the Mn_2O_3-like surface exposing cations in a 3+ oxidation state, a single desorption feature is observed in Fig. 4(c) with a peak maximum at 190 K. This desorption temperature is similar to the lower temperature feature from the Mn_3O_4-like surface. Considering that the two surfaces both likely expose surface Mn^{3+} cations, the feature near 190 K is attributed to desorption from surface Mn^{3+} cations. This conclusion is also consistent with the mixed Mn oxidation states (2+ and 3+) in Mn_3O_4.

Fig. 4(d) shows the water TPD traces on the $NaMnO_2$-like surface. A single desorption peak at 182 K is observed, similar to that seen for the Mn_2O_3-like surface. This result is consistent with the expected Mn^{3+} oxidation state in $NaMnO_2$. Therefore, water TPD appears to be sensitive to surface Mn cations in different oxidation states, and confirms the Mn^{3+} oxidation state for the $NaMnO_2$-like surface.

We note that this interpretation of the water TPD from the $NaMnO_2$-like surface implies that the Na^+ sites are either inaccessible or negligibly bind water. Our water TPD data do not distinguish between these two possibilities. However, sodium-manganese oxides are layered compounds with Na^+ located between sheets of MnO_6 octahedra [42, 43], so the possibility exists that Na^+ is buried between MnO_2 layers and inaccessible to water. The CO_2 TPD data (below) suggest that this is the case.

4.4. CO_2 and D_2O TPD on the $NaMnO_2$-like surface

A TPD study of the interactions between CO_2, water and the $NaMnO_2$-like surface was performed in the hopes of gaining insight into the mechanism of Na^+ extraction from aqueous CO_2. TPD traces for 0.5 L CO_2, 0.5 L D_2O and sequential 0.5 L CO_2 and 0.5 L D_2O doses in both orders on the $NaMnO_2$-like surface are shown in Fig. 5. For each run, the surface was cooled to 125 K before gas exposure, then TPD was run for the temperature range from 125 K to 600 K. For CO_2 alone in Fig. 5(a), the primary CO_2 desorption features are below 300 K, indicating that Na in the $NaMnO_2$-like surface does not strongly bind CO_2, in contrast to observations for oxidic sodium adatoms (Na^+) on MnO(100) seen in our earlier work [17]. This result suggests that Na in our $NaMnO_2$ layer is not accessible at the surface. For D_2O alone in Fig. 5(b), the single D_2O desorption feature at 182 K is associated with surface Mn^{3+} as discussed in section 4.3. For sequential D_2O and CO_2 doses, when D_2O is dosed prior to CO_2 as shown in Fig. 5(c), the CO_2 desorption features are significantly attenuated compared to that for CO_2 alone on the $NaMnO_2$-like surface, while the D_2O desorption features show no significant difference compared to that for D_2O alone on the $NaMnO_2$-like surface. These results suggest that water blocks the uptake of CO_2 on the $NaMnO_2$-like surface. Similar TPD results are

observed when CO_2 is dosed prior to D_2O, indicating that water displaces pre-adsorbed CO_2 from the $NaMnO_2$-like surface.

In the recovery steps of the reported thermochemical water splitting cycle [5], CO_2 is bubbled through an aqueous suspension of $NaMnO_2$ at 80°C to extract Na^+ from $NaMnO_2$ to form Na_2CO_3 and protonic birnessite-type manganese oxides ($H_xMnO_2 \cdot yH_2O$). In our work on the formation of Na_2O and Na_2CO_3 on MnO(100) [44], the decomposition of Na_2CO_3 on MnO(100) gives rise to a high temperature CO_2 TPD desorption peak around 800 K. However in this study, the majority of adsorbed CO_2 on the $NaMnO_2$-like surface desorbs below 300 K with no high temperature (> 300 K) CO_2 desorption peak observed, suggesting no strong interaction between water, CO_2 and Na in $NaMnO_2$ under the conditions of our study, and no sign of the formation of Na_2CO_3. In our study of sequential CO_2 and water doses on MnO(100) [45], water is found to stabilize pre-adsorbed CO_2 near surface defects on MnO(100), leading to an increase in temperature of the CO_2 desorption to 400 K, presumably resulting from the decomposition of bicarbonate species. However a similar stabilization is not observed on the $NaMnO_2$-like surface, suggesting no strong interactions between CO_2 and Na in the presence of water on the $NaMnO_2$-like surface and no formation of sodium bicarbonate. These results for $NaMnO_2$ indicate that our simple TPD study with D_2O and CO_2 adsorption at low temperature in UHV provides no real insight into the mechanism of Na^+ extraction by aqueous CO_2 seen in the study of Davis and coworkers [5]. Given that carbon dioxide and water desorb primarily below 300 K in our study, it is likely that the activation barrier for water intercalation to enhance the Na^+ mobility for the extraction reaction [5] exceeds those for the simple desorption of CO_2 and D_2O in our TPD experiments.

5. Conclusions

Mn_3O_4-like and Mn_2O_3-like surfaces can be formed in UHV by the oxidation of the clean and nearly-stoichiometric MnO(100). A $NaMnO_2$-like surface can be produced by oxidation of the MnO(100) pre-covered by a high coverage of metallic Na. No long range order is observed for these oxidized surfaces. Water is sensitive to Mn oxidation state, and desorbs at different temperatures from the manganese oxide surfaces dependent on the Mn oxidation state. On the $NaMnO_2$-like surface, pre-adsorbed water blocks the uptake of CO_2, and water displaces pre-adsorbed CO_2.

Acknowledgement

The authors gratefully acknowledge financial support by the Chemical Sciences, Geosciences and Biosciences Division, Office of Basic Energy Sciences, Office of Science, U.S. Department of Energy through Grant DE-FG02-97ER14751, and private support from Mr. and Mrs. Lewis W. van Amerongen.

References

[1] O.I. Velikokhatnyi, C.C. Chang, P.N. Kumta, Phase stability and electronic structure of $NaMnO_2$, Journal of The Electrochemical Society, 150 (2003) A1262-A1266.

[2] X. Ma, H. Chen, G. Ceder, Electrochemical properties of monoclinic $NaMnO_2$, Journal of The Electrochemical Society, 158 (2011) A1307-A1312.

[3] J.-P. Parant, R. Olazcuaga, M. Devalette, C. Fouassier, P. Hagenmuller, Sur quelques nouvelles phases de formule NaxMnO2 ($x \leqslant 1$), Journal of Solid State Chemistry, 3 (1971) 1-11.

[4] S.-i. Hirano, R. Narita, S. Naka, Hydrothermal synthesis and properties of $NaxMnO_2$ crystals, Journal of Crystal Growth, 54 (1981) 595-599.

[5] B. Xu, Y. Bhawe, M.E. Davis, Low-temperature, manganese oxide-based, thermochemical water splitting cycle, Proceedings of the National Academy of Sciences, 109 (2012) 9260-9264.

[6] M. Oku, K. Hirokawa, S. Ikeda, X-ray photoelectron spectroscopy of manganese-oxygen systems, Journal of Electron Spectroscopy and Related Phenomena, 7 (1975) 465-473.

[7] M. Oku, K. Hirokawa, X-ray photoelectron spectroscopy of Co_3O_4, Fe_3O_4, Mn_3O_4, and related compounds, Journal of Electron Spectroscopy and Related Phenomena, 8 (1976) 475-481.

[8] J.S. Foord, R.B. Jackman, G.C. Allen, An X-ray photoelectron spectroscopic investigation of the oxidation of manganese, Philos. Mag. A, 49 (1984) 657-663.

[9] V. Di Castro, G. Polzonetti, XPS study of MnO oxidation, Journal of Electron Spectroscopy and Related Phenomena, 48 (1989) 117-123.

[10] V. Bayer, R. Podloucky, C. Franchini, F. Allegretti, B. Xu, G. Parteder, M.G. Ramsey, S. Surnev, F.P. Netzer, Formation of Mn_3O_4(001) on MnO(001): Surface and interface structural stability, Physical Review B, 76 (2007) 165428.

[11] M.A. Langell, C.W. Hutchings, G.A. Carson, M.H. Nassir, High resolution electron energy loss spectroscopy of MnO(100) and oxidized MnO(100), J Vac Sci Technol A, 14 (1996) 1656-1661.

[12] G.V. Gibbs, N.L. Ross, D.F. Cox, K.M. Rosso, B.B. Iversen, M.A. Spackman, Bonded Radii and the Contraction of the Electron Density of the Oxygen Atom by Bonded Interactions, J. Phys. Chem. A, 117 (2013) 1632-1640.

[13] V.E. Henrich, P.A. Cox, The surface science of metal oxides, Cambridge University Press, Cambridge, NY, 1994.

[14] N.N. Greenwood, A. Earnshaw, Chemistry of the Elements (2nd Edition), Elsevier, 1997.

[15] M. Prutton, J.A. Walker, M.R. Welton-Cook, R.C. Felton, J.A. Ramsey, LEED studies of the structures of the (100) surfaces of divalent metal oxides, Surface Science, 89 (1979) 95-101.

[16] R.L. Summers, NASA Technical Note TN D-5285, in, Washington, D. C., 1969.

[17] X. Feng, D.F. Cox, Na Deposition on MnO(100), Surface Science, 645 (2016) 23-29.

[18] D.A. Shirley, High-Resolution X-Ray Photoemission Spectrum of the Valence Bands of Gold, Phys. Rev. B, 5 (1972) 4709-4714.

[19] D. Kanama, S.T. Oyama, S. Otani, D.F. Cox, Photoemission and LEED characterization of Ni_2P(0001), Surf. Sci., 552 (2004) 8-16.

[20] C.D. Wagner, L.E. Davis, M.V. Zeller, J.A. Taylor, R.H. Raymond, L.H. Gale, Empirical atomic sensitivity factors for quantitative analysis by electron spectroscopy for chemical analysis, Surf. Interface Anal., 3 (1981) 211-225.

[21] J.J. Yeh, I. Lindau, Atomic subshell photoionization cross sections and asymmetry parameters: $1 \leqslant Z \leqslant 103$, At. Data Nucl. Data Tables, 32 (1985) 1-155.

[22] S. Tanuma, C.J. Powell, D.R. Penn, Calculations of electron inelastic mean free paths. V. Data for 14 organic compounds over the 50-2000 eV range, Surf. Interface Anal., 21 (1994) 165-176.

[23] S. Tanuma, C.J. Powell, D.R. Penn, Calculation of electron inelastic mean free paths (IMFPs) VII. Reliability of the TPP-2M IMFP predictive equation, Surf. Interface Anal., 35 (2003) 268-275.

[24] C.J. Powell, A. Jablonski, NIST Electron Inelastic-Mean-Free-Path Database - Version 1.2, National Institute of Standards and Technology, Gaithersburg, MD, 2010.

[25] F. Müller, R. de Masi, D. Reinicke, P. Steiner, S. Hüfner, K. Stöwe, Epitaxial growth of MnO/Ag(001) films, Surface Science, 520 (2002) 158-172.

[26] L.Z. Zhao, V. Young, XPS studies of carbon supported films formed by the resistive deposition of manganese, J. Electron. Spectrosc. Relat. Phenom., 34 (1984) 45-54.

[27] C.S. Fadley, D.A. Shirley, Multiplet splitting of metal-atom electron binding energies, Physical Review A, 2 (1970) 1109-1120.

[28] P. Steiner, R. Zimmermann, F. Reinert, T. Engel, S. Hüfner, 3s- and 3p-core level excitations in 3d-transition metal oxides from electron-energy-loss spectroscopy, Z. Phys. B: Condens. Matter, 99 (1996) 479-490.

[29] X. Feng, Interactions of Na, O_2, CO_2 and water with MnO(100): modeling a complex mixed oxide system for thermochemical water splitting, in: Chemical Engineering, Virginia Polytechnic Institute and State University, 2015, pp. 118.

[30] M. Bender, K. Al-Shamery, H.J. Freund, Sodium adsorption and reaction on NiO(111)/Ni(111), Langmuir, 10 (1994) 3081-3085.

[31] H. Onishi, C. Egawa, T. Aruga, Y. Iwasawa, Adsorption of Na atoms and oxygen-containing molecules on MgO(100) and (111) surfaces, Surface Science, 191 (1987) 479-491.

[32] J.F. Moulder, W.F. Stickle, P.E. Sobol, K.D. Bomben, Handbook of X-ray photoelectron spectroscopy, Perkin-Elmer Corporation, Eden Prairie, MN, 1992.

[33] A. Barrie, F.J. Street, An Auger and X-ray photoelectron spectroscopic study of sodium metal and sodium oxide, Journal of Electron Spectroscopy and Related Phenomena, 7 (1975) 1-31.

[34] C.D. Wagner, W.M. Riggs, L.E. Davis, J.F. Moulder, G.E. Muilenberg, Handbook of X-ray photoelectron spectroscopy, Perkin-Elmer Corporation, Eden Prairie, MN, 1978.

[35] F. Wu, G. Yu, D. Xu, E. Kan, First-principles investigations on the magnetic structure of α-$NaMnO_2$, Journal of Physics: Condensed Matter, 24 (2012) 456002.

[36] M.J. Stirniman, C. Huang, R. Scott Smith, S.A. Joyce, B.D. Kay, The adsorption and desorption of water on single crystal MgO(100): The role of surface defects, J. Chem. Phys., 105 (1996) 1295-1298.

[37] C. Xu, D.W. Goodman, Structure and geometry of water adsorbed on the MgO(100) surface, Chem. Phys. Lett., 265 (1997) 341-346.

[38] R. Reissner, M. Schulze, Multilayer adsorption of water on NiO(100) at 120 and 143K, Surf. Sci., 454-456 (2000) 183-190.

[39] M. Schulze, R. Reissner, Adsorption of water on epitactic NiO(100), Surf. Sci., 482-485 (2001) 285-293.

[40] M.A. Henderson, The interaction of water with solid surfaces: fundamental aspects revisited, Surf. Sci. Rep., 46 (2002) 1-308.

[41] P.A. Thiel, T.E. Madey, The interaction of water with solid surfaces: Fundamental aspects, Surf. Sci. Rep., 7 (1987) 211-385.

[42] Q. Feng, H. Kanoh, K. Ooi, Manganese oxide porous crystals, J. Mater. Chem., 9 (1999) 319-333.

[43] A. Mendiboure, C. Delmas, P. Hagenmuller, Electrochemical intercalation and deintercalation of Na_xMnO_2 Bronzes, Journal of Solid State Chemistry, 57 (1985) 323-331.

[44] X. Feng, D.F. Cox, O_2 Adsorption on Na-precovered MnO(100): XPS and CO_2 Characterization, In Preparation.

[45] X. Feng, H. Chen, D.F. Cox, CO_2 and Water Adsorption on MnO(100), In Preparation.

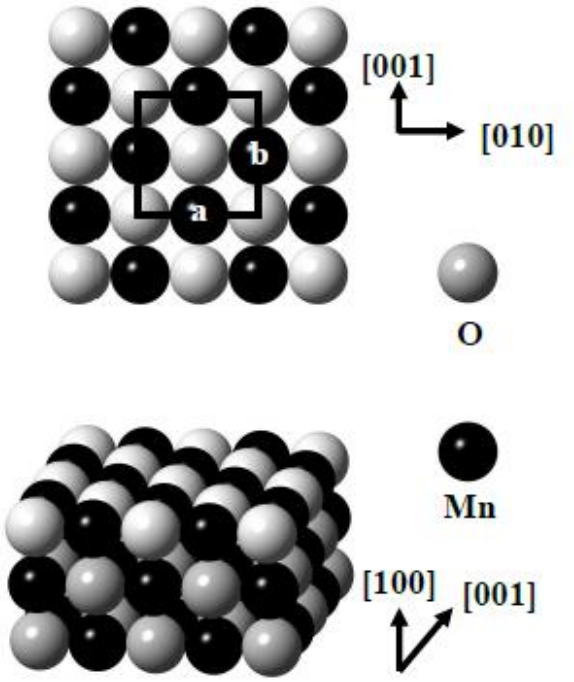

Figure 1. Ball model illustration of the ideal stoichiometric MnO(100) surface. Grey spheres represent O^{2-} anions, and black spheres represent Mn^{2+} cations. Atom sizes are referenced to Mn and O bonded radii [12]. Surface O^{2-} anions on the (100) plane are marked with lighter grey color for clarity. The top picture shows the surface periodicity (a:b = 1:1) looking down the [100] surface normal. The bottom picture shows a cross-section view along the [001] direction.

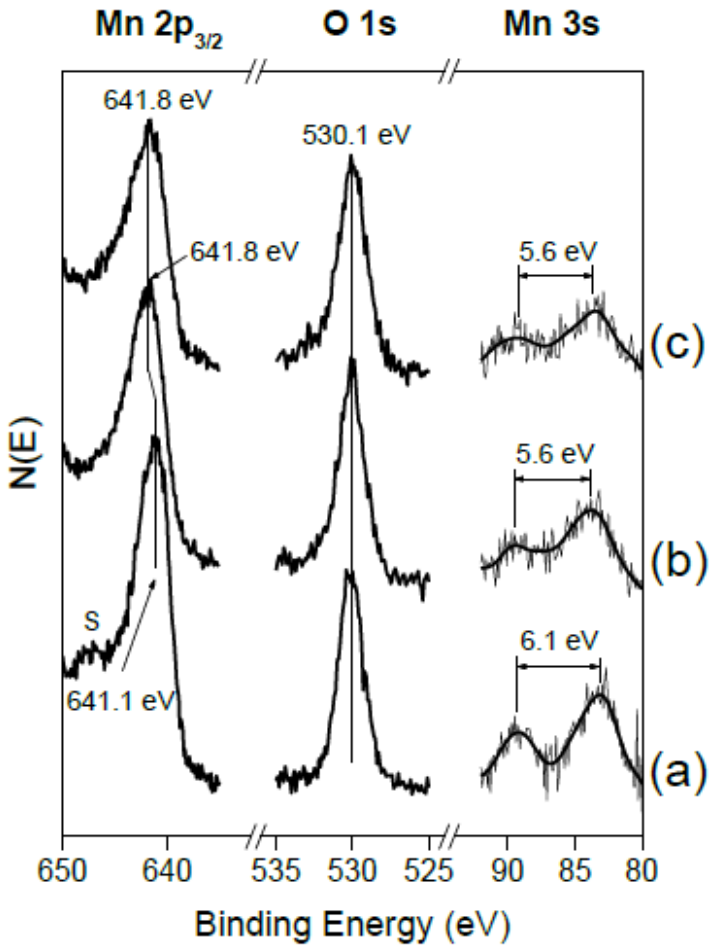

Figure 2. Mn $2p_{3/2}$, Mn 3s and O 1s XPS spectra of (a) the clean and nearly-stoichiometric MnO(100); (b) the Mn_3O_4-like surface; (c) the Mn_2O_3-like surface. Curves for the Mn 3s spectra smoothed using an FFT filter are also shown. Symbol S represents the shake-up satellite feature of Mn $2p_{3/2}$.

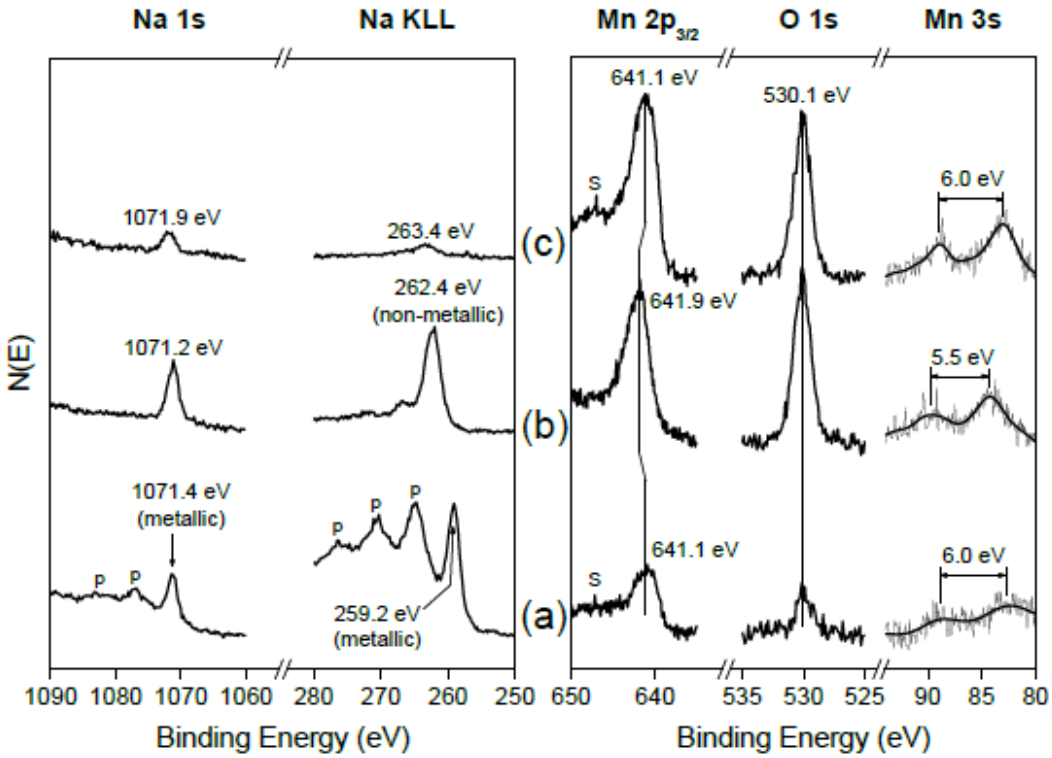

Figure 3. Na 1s and KLL, Mn $2p_{3/2}$ and 3s and O 1s XPS spectra of (a) 11.5 ML Na-precovered MnO(100); (b) the $NaMnO_2$-like surface; (c) the $NaMnO_2$-like surface after prolonged UHV annealing (> 10 min) at 1000 K. Curves for the Mn 3s spectra smoothed using an FFT filter are also shown. Symbol p represents the plasmon loss features of metallic Na and symbol S represents the shake-up satellite feature of Mn $2p_{3/2}$.

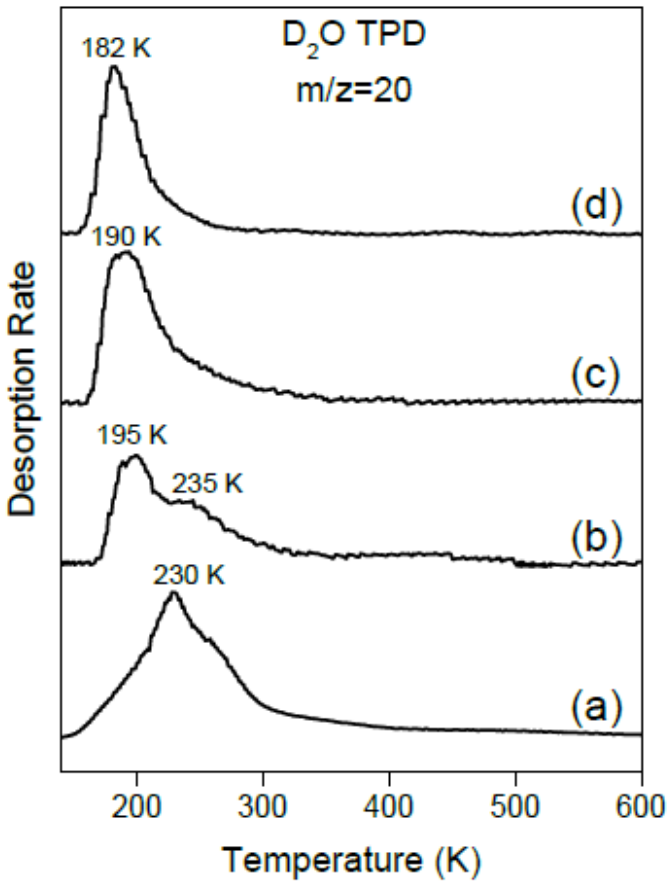

Figure 4. TPD traces of D_2O (m/z = 20) following 0.5 L D_2O adsorption on (a) the clean and nearly-stoichiometric MnO(100); (b) the Mn_3O_4-like surface; (c) the Mn_2O_3-like surface; (d) the $NaMnO_2$-like surface.

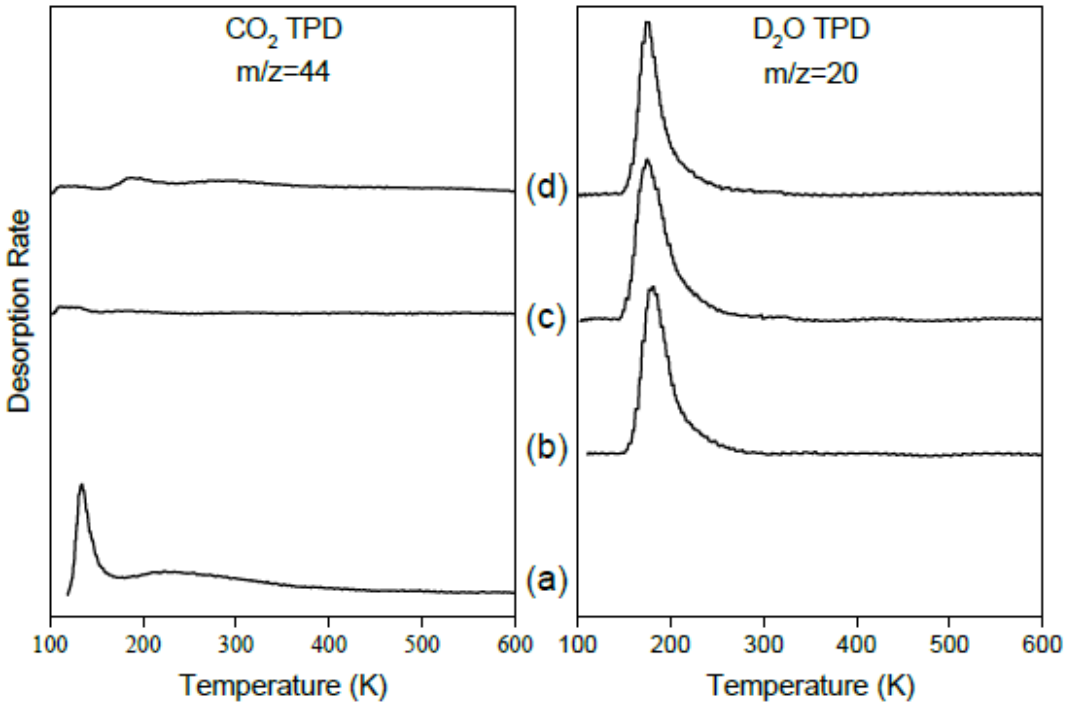

Figure 5. TPD traces of CO_2 (m/z = 44) and D_2O (m/z = 20) from the $NaMnO_2$-like surface following (a) a 0.5 L CO_2 dose; (b) a 0.5 L D_2O dose; (c) a 0.5 L CO_2 dose following a 0.5 L D_2O pre-dose; (d) a 0.5 L D_2O dose following a 0.5 L CO_2 pre-dose.

Graphical Abstract